

PHYSICO-CHEMICAL STUDIES OF THE INTERACTION MECHANISM OF DOUBLE AND TRIVALENT IRON DOUBLE OXIDE NANOPARTICLES WITH SERPIN PROTEIN OVALBUMIN AND WATER

Iryna Tsykhanovska¹, Mykola Riabchykov², Olexandr Alexandrov¹, Victoriya Evlash³, Oksana Bryzyska⁴, , Sergey Gubsky³, Tatyana Lazareva¹, Olga Blahyi¹

<https://doi.org/10.23939/chcht17.03.481>

Abstract. The novelty of the work is the theoretical justification and experimental confirmation of the mechanism of interaction of Fe₃O₄ nanoparticles with H₂O and ovalbumin-OVA, which was carried out with the help of a complex of physical and chemical studies. It was determined that the mechanism is based on the clusterophilicity of nanoparticles and hydrogen, electrostatic and van der Waals interactions. It was established that the interaction of Fe₃O₄ nanoparticles with OVA took place by the mechanism of static quenching with the formation of an intermolecular non-fluorescent complex that changes the native structure of OVA. The binding constant varied from 3.3×10^5 to 4.8×10^5 L·mol⁻¹ depending on the pH value of the medium and temperature. Thermodynamic calculations confirmed the spontaneity of the binding process with the predominance of the enthalpy factor.

Keywords: Fe₃O₄ nanoparticles, water, OVA, binding, water absorption, water retention.

1. Introduction

A polyphase structure is characteristic of a wide range of products of the national economic complex. Accordingly, various products of the agro-industrial industry have a multi-component heterogeneous structure. Therefore, the problem of stabilization of polyphase “lyophilic colloids” is urgent. The approach to the stabilization of lyophilic colloid-dispersed systems from a

chemical point of view, and in particular, colloid chemistry, is based on the functional and technological properties of the chemicals that make up these systems: proteins, carbohydrates, lipids, lipoproteins, H₂O, *etc.* That is caused by the spatial location and interaction of the system's constituent parts.¹ Studying the interaction of components of dispersed systems is one of the crucial stages in developing innovative industrial technologies.² However, due to the multicomponent composition of the dispersed matrix, it is practically impossible to predict the functional effect of its components.³ One of the key structure-forming components of colloidal dispersion systems is proteins of plant or animal origin. Each type of protein has different functional properties, such as solubility, structure formation, emulsification, gel and foam formation, viscosity increase, binding, and retention of water molecules.^{2,3}

The use of nanomaterials is a promising area of innovative development of industrial technologies. The interaction of nanoparticles with biopolymers of dispersed systems (proteins, carbohydrates, lipoproteins) is a complex of complex chemical interactions, where the supramolecular organization of nanoparticles and the structure of the organic matrix play an essential role.^{4,5} As a result of this process, spatial nanostructures are formed, which significantly affect the functional and technological properties of the constituent components of heterogeneous systems.⁶ Important information for understanding these processes can be obtained by studying the nature and strength of the interaction of nanoparticles with chemical substances of colloidal dispersion systems.⁷ This approach provides a basis for understanding the interaction and behavior of chemical substances during the formation of a micromatrix, which affects the functional properties on a macroscopic scale.⁸

Currently, a number of studies has been conducted on the use of Fe₃O₄ nanoparticles in innovative industrial production.⁹ This component has a nanometer size, stable physical and chemical characteristics, and high functional and technological potential.

¹ Ukrainian Engineer Pedagogic Academy, Universitetska St., 16, 61003, Kharkiv, Ukraine

² Lutsk National Technical University, Lvivska St., 75, 43018, Lutsk, Ukraine

³ State Biotechnological University, Klochkivska St., 333, 61051, Kharkiv, Ukraine

⁴ National University of Pharmacy, Pushkinska St., 53, 61002, Kharkiv, Ukraine

 oksanabrizi69@gmail.com

© Tsykhanovska I., Riabchykov M., Alexandrov O., Evlash V., Bryzyska O., Gubsky S., Lazareva T., Blahiy O., 2023

It is used to adjust the functional and technological properties of raw materials (stabilizing, water- and fat-binding abilities) and to improve the quality of finished products.¹⁰⁻¹² In addition, to increase water and fat binding, water and fat retention; improving the stabilization of polyphase systems using ZnO nanoparticles applied to a carboxymethylcellulose film; AgNPS, micro- and nano-sized powders of various origins, modified nanocomposite (CNS-nZVI) with high adsorption capacity¹³⁻¹⁵ are used. The expediency of their use is determined by a wide range of functional and technological properties, thanks to high dispersion, shape, structure, and physicochemical indicators.

Thus, the problem of stabilization of the polyphase structure, in particular, due to complex structure formation, water binding, and water retention, is actual. Knowledge of the mechanisms of binding and retention of water by chemical substances, in particular proteins, carbohydrates, lipoproteins, *etc.*, allows to rationally use new types of raw materials and predict the behavior of its components in dispersed systems during technological processing and during use and storage of finished products. To improve the technological process and optimize its manageability, the following points are of great importance: knowledge of the mechanisms of hydrophilic interaction of basic chemical substances (proteins, carbohydrates, lipids); regulation of moisture sorption-desorption processes using technological parameters (temperature, acidity, *etc.*) and technological methods (introduction of biologically active and other substances).

Since the process of stabilizing, water-binding and water-holding capacities by nanoparticles of double oxide of bi- and trivalent ferrum (Fe_3O_4) and the mechanism of their interaction with protein molecules are not sufficiently investigated and substantiated, in this paper we present studies that are related to determining the nature of the interaction of Fe_3O_4 nanoparticles with H_2O and the sickle series protein – ovalbumin-OVA.

The aim of the research is to study the mechanism of interaction of Fe_3O_4 nanoparticles with H_2O and with OVA.

2. Experimental Part

2.1. The Studied Samples Used in the Experiment

Research subjects:

Selection of the research subject: nanoparticles of the double oxide of di- and trivalent ferrum (Fe_3O_4) and OVA were chosen because they are the most promising chemicals in terms of improving the stabilizing and structure-forming abilities of polyphase systems. In

addition, ovalbumin OVA is quite popular in a number of technologies.

– sample 1 – highly dispersed Fe_3O_4 powder from dark brown to black in color with particle size $\langle d \rangle < 70$ nm. were obtained according to the technology improved by the authors, which is based on the reaction of chemical coprecipitation of iron salts in an alkaline medium.⁸⁻¹⁰ Initial suspensions of Fe_3O_4 nanoparticles (NP Fe_3O_4) were obtained by dispersing the calculated amount of NP Fe_3O_4 in deionized water with pH=7.8 (adjusted with NaOH and HCl) at a temperature of 291...293 K for $(5...7) \times 60$ s, followed by holding for $(10...12) \times 60$ s. Analyses were held using dynamic light scattering (DLS) and ζ -potential;

– sample 2 – OVA (Ovostar, UA company). Ovalbumin-OVA stock solution (4 μM) was prepared in 100 mM HCl solution (pH adjusted to 1.5) containing 100 mM NaCl, and working solutions were prepared by further appropriate dilution. The concentration of ovalbumin-OVA was determined by the spectrophotometric method at $\lambda=280$ nm (molar extinction coefficient – $30957 \text{ M}^{-1}\text{cm}^{-1}$) after appropriate dilution of the solution;

– sample 3 – “OVA+NPF Fe_3O_4 ” suspension, which was obtained by introducing the calculated amount of NPF Fe_3O_4 into a 3% solution of ovalbumin-OVA at a temperature of (291...293) K with constant stirring $n = (2.0...2.2) \text{ s}^{-1}$ during $(3...5) \times 60$ s followed by holding for $(5...7) \times 60$ s.⁹

2.2. Methods of Investigation

2.2.1. Infrared Fourier spectroscopy (FTIR)

The vibrational spectra of the studied samples were obtained by the IR-Fourier spectroscopy method on the Tensor 37 Fourier spectrometer of the Bruker company (Germany), controlled by the OPUS software package with standard calibration capabilities in the frequency range (4000–400) cm^{-1} in the absorption format (IR–Fourier spectra were recorded in KBr tablets).¹²

2.2.2. Dynamic Light Scattering (DLS)

The values of the ζ -potential and hydrodynamic radius of OVA, NPF Fe_3O_4 and the OVA/NPF Fe_3O_4 system (1:1 mass ratio) were performed using dynamic light scattering (DLS) (Zetasizer Nano ZS, Malvern Instruments, UK) in two media: double distilled water (DDW) (pH ≤ 7) and phosphate buffer solution (PBS, 100 mM, pH=7.4) at a temperature of 296 K.^{9,16}

2.2.3. Fluorescence Spectroscopy

Molecular fluorescence was measured on a SOLAR SM 2203 spectrofluorimeter (JSC SOLAR, belarus) using quartz cuvettes with an optical path of 10 mm, height of 45 mm, width of 12.5 mm, and depth of

12.5 mm with four polished windows and a camera volume is 3.5 mL. Fluorescence spectra of OVA (2.0 μM) in the absence and presence of NPFe_3O_4 (2.0...100.0 μM) were recorded from 250 nm to 450 nm with $\lambda_{\text{ex}}=280$ nm. The width of the slits of the excitation and emission channels was 4 nm and 7 nm, respectively. All fluorescence analyses were performed at $\text{pH}=4.6$; $\text{pH}=7.4$ and temperatures of 296 K and 311 K.^{9,16,17}

The concentration of OVA in the phosphate buffer ($\text{pH}=7.8$, 50 mM) was fixed at 2 μM , and changes in the fluorescence intensity of OVA were recorded in samples with different concentrations of NPFe_3O_4 in the range of: 2, 4, 8, 15, 30, 50 and 100 μM .

2.2.4. Energy Dispersive X-Ray Spectroscopy (EDX)

A scanning electron microscope JSM-820 (JEOL) with an EDX attachment was used to determine the elemental composition of the studied samples 1–3. X-ray spectra were obtained by bombarding the studied samples with electrons using an acceleration voltage of 20 kV (corresponding to the lines of the characteristic spectra of Iron, Carbon, Oxygen, Nitrogen, Sulfur, Potassium, Sodium, and Chlorine). The elemental composition of the studied samples was determined by analyzing the obtained spectra of characteristic X-ray radiation. Lyophilized samples 2, 3 were analyzed according to the methodology.¹⁸ Liquid samples 2, 3 in the amount of 12 mL were placed in test tubes covered with a polyethylene film and paraffin. In which holes were made with a needle. Then it was frozen at a temperature of 203 K for 4 hours. Next, the test tubes with the samples were transferred to a lyophilizer and dried (sublimated) at a temperature of (293...298) K for 45 hours. Dried samples were used for analysis.^{11,17}

2.2.5. Water Absorption Coefficient (Degree of Swelling) NPFe_3O_4

The degree of swelling (Q , %) was determined on the Dogadkin device at two temperatures: (293 \pm 5K) and (323 \pm 8K) in technological environments¹⁸ according to the formula (1):

$$Q = \frac{M_H}{M_o} \times 100 = \frac{\rho V}{M_o} \times 100, \quad (1)$$

where M_o is the weight of the weight before swelling, g; M_H is the weight of the sample after swelling, g; ρ is the density of the absorbed liquid, g/cm^3 ; V is the volume of absorbed liquid, cm^3 ($V=2 \cdot Dh \cdot K_p$); h is the height of the absorbed liquid column, cm; D is a tube diameter, cm; K_p is a coefficient of the device.

2.2.6. Water Absorption Capacity (WAC) of NPFe_3O_4 . Weight Method

The technique is based on the binding of water at $T=293$ K by the NPFe_3O_4 hydromodule, followed by centrifugation and determination of the WAC (α_m , %) by the standard weight method¹⁸ according to formula (2):

$$\alpha_m = \frac{m - m_o}{m_o}, \quad (2)$$

where m_o and m are the weight of NPFe_3O_4 before and after solvation.

2.2.7. Water Absorption Capacity (WAC) of NPFe_3O_4 . Indicator Refractometric Method

It consists in determining the difference in dry matter between solutions of "indicator" sugar and NPFe_3O_4 , solvated in a sugar solution.^{4,10,19} The bound moisture was determined according to formula (3):

$$X = \frac{B \times (b_2 - b_1)}{P \times b_2}, \quad (3)$$

where X is the amount of bound water, g per 1 g of dry matter; b_1 and b_2 are initial and final concentrations of sucrose solution %; B is a mass of 20 cm^3 of 10 % sucrose solution, g; P is the weight of dry matter, g.

Free moisture was determined by formula (4):

$$Y = \frac{(C_0 - C_1) \times m \times 100}{C_1 \times g \times W}, \quad (4)$$

where Y is the content of free water, % of the total content; C_0 , C_1 are initial and final concentrations of sucrose solution, %; m is the mass of the original sucrose solution, g; g is the weight, g; W is the total water content in 1 g of the sample, g.

2.2.8. Differential Thermal Analysis (DTA)

Thermographic determinations were carried out on the Q-1500D derivatograph of the MOM company (Hungary) for a weighing weight of 0.5 g under the following derivatogram recording modes: sensitivity of DTA-250 galvanometer, DTG-500 galvanometer, TG-500 galvanometer, rate of change of heating temperature – 277 K/60 s.¹² Based on the change in the TG curve, which corresponds to the dehydration process, the temperature T curve, the dependence of the degree of mass change α on the temperature T was constructed. For this purpose, the change in the mass of the sample corresponding to the mass fraction of moisture removed at the temperature T was found on the TG curve every 278 K, as well as the total mass fraction of moisture, which was determined by the TG curve at the end of the dehydration process. The degree of mass change α was calculated according to the formula (5):

$$\alpha = \frac{\Delta m_T}{m}, \quad (5)$$

where α is the degree of mass change, Δm_T is the change in mass of the sample at temperature (T), 10^{-3} g; m is the total mass fraction of moisture contained in the sample, 10^{-3} g.

2.2.9. Swelling NPFe₃O₄

Swelling was determined by infusing a 1% aqueous suspension of the NPFe₃O₄ test sample for a day. Swelling capacity (cm³/g) was estimated as the maximum amount of water that the object can absorb and hold until the moment of dynamic equilibrium, related to the mass of the weight.^{4,10,19}

2.2.10. Moisture Retention Capacity (MRC) NPFe₃O₄

Moisture retention capacity was determined by the Shokh method as the amount of water adsorbed and retained by the raw material component during the infusion and centrifugation of the aqueous suspension.^{4,10,19}

3. Results and Discussion

3.1. Justification of the Mechanism of Interaction of OVA with Nanoparticles of Fe₃O₄

3.1.1. Determination of ζ -Potential and Hydrodynamic Radius

ζ -Potential characterizes the stability of dispersed systems. A higher electric charge on the surface of the particles reduces their tendency to aggregate due to strong repulsive forces between them. Suppose the value of ζ -potential is above 30 mV, in the range of 5 mV to 30 mV, and below 5 mV. In that case, it indicates good stability, short-term stability, and rapid particle aggregation, respectively.

The effect of Fe₃O₄ nanoparticles (NPFe₃O₄) on the surface charge and dispersion of particles in the OVA/

NPFe₃O₄ system was investigated using the ζ -potential and dynamic light scattering (Table 1).

The data in Table 1 show an increase in the ζ -potential of the OVA/NP Fe₃O₄ dispersed system by 1.89...1.92 times compared to OVA. At the same time, the ζ -potential of the OVA/NPFe₃O₄ system has a rather high value, which is consistent with the works of other authors.^{9,20} This fact determines the possibility of stabilizing dispersed systems based on OVA with Fe₃O₄ nanoparticles. The interaction of OVA with NPFe₃O₄ leads to an increase in the electrokinetic potential of the OVA/NPFe₃O₄ system (due to an increase in surface charge values and prevention of aggregation). The increase in the size of NPFe₃O₄ in solution to 77...78 nm compared to the nominal ($\langle d \rangle > 70$ nm) is due to the formation of a surface layer of H₂O molecules on the surface of NPFe₃O₄. At the same time, in an acidic environment, Fe₃O₄ nanoparticles more intensively enter into chemical interactions with H₂O dipoles and ionogenic groups of OVA, while interactions in solvato- and peptido complexes are strengthened.^{4,5,12}

The effectiveness of the stabilization of dispersed NPFe₃O₄ systems is explained by the formation of a double electrical surface layer.²¹ In the OVA/NPFe₃O₄ system, Fe₃O₄ nanoparticles are located at the boundary of the OVA/H₂O phase distribution, with the formation of a monomolecular solvate layer consisting of water molecules that are retained on the surface of the dispersed phase (solid NPFe₃O₄) due to chemisorption processes. OVA molecules are oriented around this layer, creating a protein shell, while the surface tension at the boundary of the phase distribution decreases, which leads to an increase in the aggregative stability of the colloidal system. In addition, due to the action of Coulomb forces of repulsion of equally charged particles, the process of increasing the aggregation resistance of the colloidal system and reducing the friction force between the particles of the dispersed phase occurs. This leads to an increase in the dispersed system stability and explains the increase in the value of the ζ -potential, as well as contributes to the spatial structuring of colloidal particles.²¹ Based on these data, it can be assumed that the interaction of NPFe₃O₄ with proteins, in particular OVA, increases the stability of colloidal-dispersed systems and contributes to their effective use.

Table 1. ζ -Potential and hydrodynamical size (d) of OVA, NPFe₃O₄, OVA/NPFe₃O₄ systems in double distilled water (DDW) (pH ≤ 7) and phosphate buffer solution (PBS) 100 mM (pH=7.4)

System	DDW (pH ≤ 7)		PBS (100 mM, pH=7.4)	
	ζ -Potential, mV	Hydrodynamical d , nm	ζ -Potential, mV	Hydrodynamical d , nm
OVA	17.52 \pm 1.14	8.91 \pm 0.37	18.22 \pm 1.16	6.69 \pm 0.21
NPFe ₃ O ₄	-32.4 \pm 1.64	78.3 \pm 2.13	-33.8 \pm 1.63	77.2 \pm 2.13
OVA/NPFe ₃ O ₄	33.2 \pm 1.62	76.2 \pm 2.09	34.9 \pm 1.67	75.3 \pm 2.09

*Note. Data represent the mean \pm standard deviation of three experiments. ($n=3$).

Table 2. Comparison of the wave numbers of individual peaks in the FTIR spectra of the complex associate OVA/NPFe₃O₄ and the starting substances (OVA, NPFe₃O₄)

Fluctuations in bonds	Position of maxima (wave numbers), cm ⁻¹			Slide, cm ⁻¹
	OVA	NPFe ₃ O ₄	OVA/NPFe ₃ O ₄	
v(O–H), v(N–H)–Amid A	3406±5	3398±5	3341±5	-(57...65)
v _{as} (C–H)	2927±4	–	2927±4	0
v _s (C–H)	–	–	2360±4; 2342±3	–
v(C=O)– Amid I	1653±3	–	1642±3	-11
δ _{pl} (O–H)	1639±3	1633±3	1625±3	-(8...14)
δ _{pl} (N–H)– Amid II	1539±3	–	1527±3	-12
δ _{pl} (C–H)	1451±3	–	1442±3	-9
δ _{pl} (C–C), δ _{pl} (C–N) – Amid III	1237±2 1244±2	–	1237±2 1240±2	– -4
δ _{pl} (C–C)	–	–	1155±2	–
δ _{non-pl} (C–C)	1079±2	–	1027±2	-52
v(Fe–O)	–	532±2	588±2	+56

3.1.2. Fourier-Transform Infrared Spectroscopy

The results of Fourier-transform infrared spectroscopic studies of OVA model systems with NPFe₃O₄ are shown in Table 2.

In an aqueous medium, the surface of NPFe₃O₄ is modified under the influence of OH⁻ groups, due to the coordination of surface water dipoles by unsaturated Fe atoms, the valence and deformation oscillations of which are manifested at ~3400 cm⁻¹ and ~1633 cm⁻¹, respectively.¹⁰ An intense broad band with an absorption maximum (3341±4) cm⁻¹ is shifted in the complex associate toward a low-frequency region compared to the vibrational frequency of bonds of free OH⁻ groups and Amide A (N–H) (3398±5; 3406±4) cm⁻¹. A similar effect is observed for the deformation vibrations of the OH group (Table 2). This fact indicates the participation of oxygen atoms of hydroxyl groups and nitrogen atoms of amide groups in the formation of coordination bonds with iron atoms in NPFe₃O₄.^{10,22}

There are also intense absorption bands with maxima at (2360±4) cm⁻¹ and (2342±3) cm⁻¹, which are absent in the OVA spectrum. These peaks can be attributed to symmetric valence (v_s) vibrations of the C–H bond, which confirms the presence of electrostatic hydrophobic interaction of aliphatic side chains of amino acid residues in “clathrates” and “cavities” arising under the action of NPFe₃O₄.^{4,10,12}

It is known that the characteristic frequencies of vibrations of the amide group of polypeptides (in particular, OVA) are observed near 1650, 1540, and 1240 cm⁻¹ (Table 2), which are generally called the vibrations “Amide I”, “Amide II” and “Amide III”, respectively.^{10,23} When OVA is adsorbed on the surface of Fe₃O₄ nanoparticles, there is a shift in the absorption

bands of the valence vibrations of Amide I v(C=O) and the plane deformation vibrations of Amide II δ_p(N–H) in the lower frequency range: v(C=O) = (1642±3) cm⁻¹; δ_p(N–H) = (1527±3) cm⁻¹, respectively.^{10,22,23}

Absorption bands of in-plane and out-of-plane deformation vibrations δ_{pl}(C–H) and δ_{inpl}(C–C) shift to a lower frequency – in the region: δ_{pl}(C–H) = (1442±3) cm⁻¹ and δ_{inpl}(C–C) = (1027±2) cm⁻¹, respectively, the appearance of a new absorption band of plane deformation vibrations δ_{inpl}(C–C) (1155±2) cm⁻¹ is also observed. This confirms the presence of electrostatic hydrophobic interaction between aliphatic and alicyclic amino acid residues in the complex associate OVA/NPFe₃O₄.^{10,17,21-23}

In the spectrum of pure NPFe₃O₄ (Table 2), there is an absorption line of the Fe–O bond with a maximum at ~532 cm⁻¹, which is in good agreement with data from literary sources at ~530 cm⁻¹.^{5,12} The shift of the maximum of the corresponding absorption band of the valence vibrations of the Fe–O bond in the OVA/NPFe₃O₄ complex to the region of ~588 cm⁻¹ is caused by the influence of OVA molecules of the surface layer, their interference with the near-surface layer of Fe₃O₄ nanoparticles, and chemisorption with iron cations. Thus, the research results confirm the existence of a process of structure formation between OVA and NPFe₃O₄.

3.1.3. Energy Dispersive Spectroscopy (EDS)

To confirm the chemisorption of OVA on the surface of Fe₃O₄ nanoparticles, the EDS method was used to determine the chemical composition of the “OVA+NPFe₃O₄” model system (Fig. 1).

In the X-ray spectra of the studied samples 1 and 3, the values of the absorption peaks are around 0.8; 6.3 and 6.8 keV and are associated with the absorption of

kinetic energy of Fe atom electrons (Fig. 1a,c). In the spectra of NPFe_3O_4 nanoparticles covered with an OVA adsorption layer (Fig. 1c), there are nine more peaks located close to: 0.22 keV; 0.25 keV; 0.27 keV; 0.30 keV; 0.47 keV; 1.0 keV; 2.4 keV; 2.6 keV and 3.25 keV. These absorption bands belong to C (0.27 keV) and O (0.47 keV) atoms.^{7,13,20} Moreover, the peak at 0.47 keV, characteristic of the O atom, is also present in the spectrum of pure NPFe_3O_4 (Fig. 1, a–c); and the peaks around 0.3 and 2.4 keV are associated with

the absorption of kinetic energy by electrons of N and S atoms, respectively. As well as the peaks at 0.22 and 3.25 keV (atom K); 1.0 keV (Na atom); 0.25 and 2.6 keV (Cl atom) are observed in the spectra of OVA and “OVA+ NPFe_3O_4 ” (Fig. 1, b–c).^{17,18}

Analysis of the EDS spectra of the test samples shows that Fe, O, and C (H cannot be investigated) and N, S, K, Na, and Cl (for sample c) are the main components in the elemental composition of the OVA/ NPFe_3O_4 system.

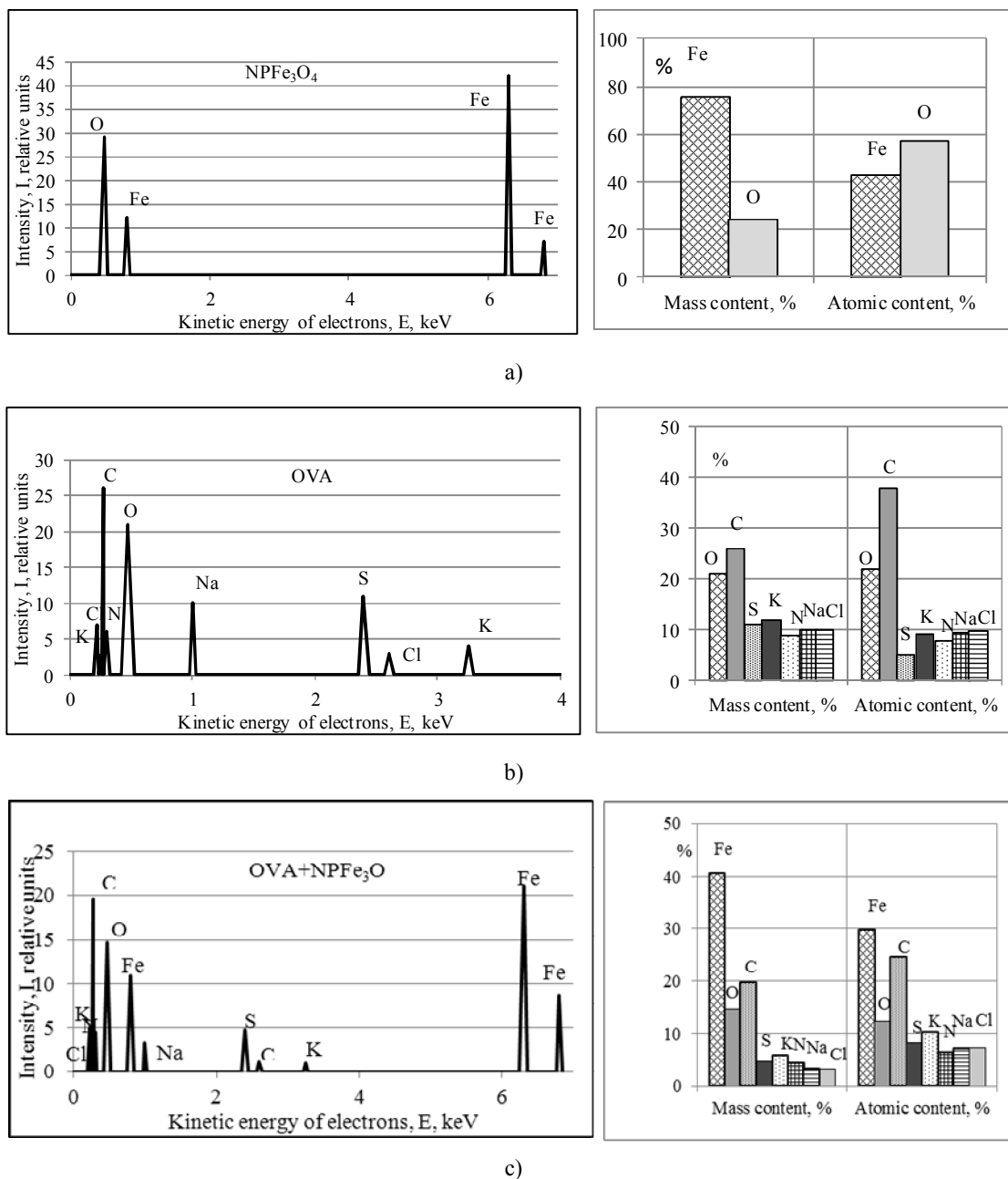


Fig. 1. EDS– spectra of model systems: *a* – NPFe_3O_4 ; *b* – OVA; *c* – “OVA+ NPFe_3O_4 ”

Thus, the investigated samples have the following chemical composition: sample *a* (NPFe₃O₄) – Fe 75.5 %; O 24.5 %; sample *b* (OVA) – Fe 0 %; O 21.0 %; C 26.0 %; N 4.4 %; S 11.4 %; K 12.0 %; Na 10.2 %; Cl 10.2 %; sample *c* ("OVA+ NPFe₃O₄") – Fe 40.7 %; O 14.7 %; C 19.6 %; N 4.4 %; S 4.7 %; K 6.0 %; Na 3.2 %; Cl 3.2 %. Therefore, a new chemical element (Fe), absent in OVA (sample *b*), and six more elements (C, N, S, K, Na, Cl), absent in pure NPFe₃O₄ (sample *a*) appear in the studied (sample *c*). The result indicates that Fe₃O₄ nanoparticles were successfully obtained (sample *a*) and OVA (sample *b*) chemisorbed on Fe₃O₄ nanoparticles.

3.1.4. Fluorescence Spectroscopy

Structural changes in OVA (in particular, the tertiary structure) caused by the effect of NPFe₃O₄ were studied by the method of fluorescence spectroscopy of tryptophan. OVA contains three tryptophan Trp residues: (the remains have different distances between the N atom of the indole fragment and the carboxyl group: Trp160, Trp194, Trp275) (Fig. 2a).^{24,25} The spectral profile of OVA emission at different concentrations of NPFe₃O₄ is shown in Fig. 2b. The intensity of fluorescent radiation in OVA is determined by pH of the medium of fluorophores. At pH = 7.4 in the spectral profile of the OVA at the first

concentrations, the intensity of fluorescence increased by 9-11 % in the depth of pH = 4.6.^{9,18} The quantum yield of Trp and, therefore, the fluorescence intensity, increases with increasing OVA concentration.

On the contrary, the quantum yield of Trp decreases (which leads to a low fluorescence intensity) in a polar hydrophilic environment or with an increase in the concentration of NPFe₃O₄.^{9,17,24} The study of the interaction of NPFe₃O₄ with OVA was carried out at pH: 4.6 (corresponds to the pH value of most technological environments, as well as the pH value of the isoelectric point of OVA – pI=4.6) and 7.4 (corresponds to the acidity of the biological environment of OVA).^{16,26}

3.1.4.1. Kinetic Study

The influence of time on the process of interaction of NPFe₃O₄ with OVA was evaluated at pH=4.6 and pH=7.4 (research time – 60 min). The fluorescence ratio (F_0/F) between the intrinsic fluorescence of the protein ($\lambda_{em}=335$ nm) (F_0) and in the presence of NPFe₃O₄ (F) was used as an analytical parameter.^{9,16} Studies have shown that the interaction between NPFe₃O₄ and OVA occurred immediately, regardless of pH. Therefore, the interaction was favorable and stable during the studied period (60 min).

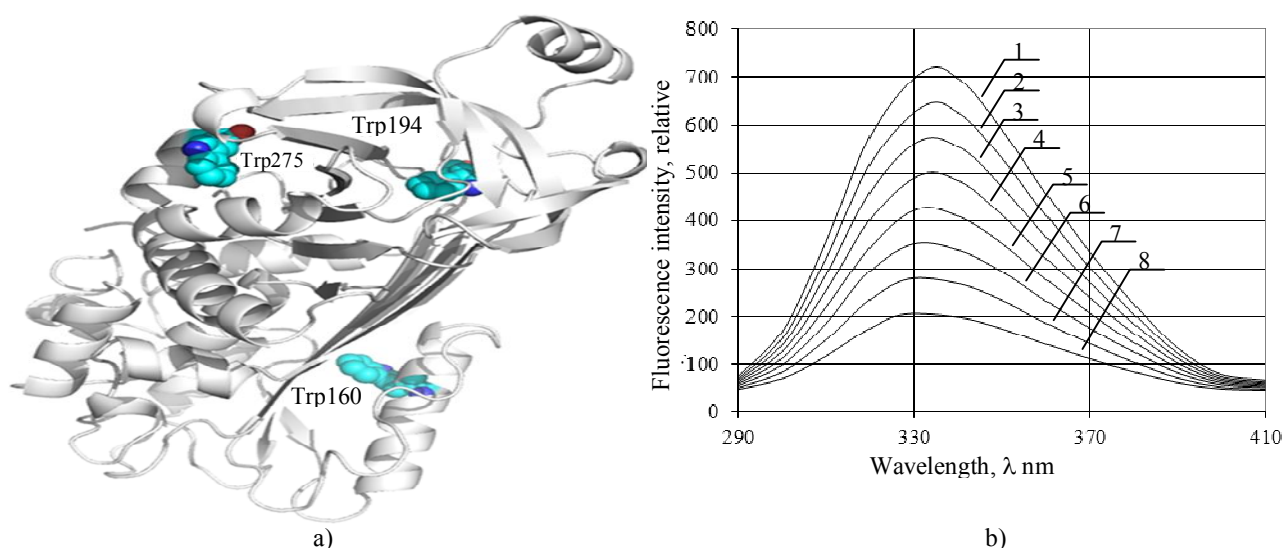


Fig. 2. Three-dimensional structure of OVA with Trp residues (a). Protein model based on OVA obtained from the Protein Data Bank (PDB)²⁵ and fluorescence quenching (b) of OVA (2 μ M) at different concentrations NPFe₃O₄ (μ M): 1– pure OVA, 2–2.0; 3–4.0; 4–8.0; 5–15.0; 6–30.0; 7–50.0; 8–100.0 (pH=4.6; temperature 296 K)

3.1.4.2. Study of the Mechanism of Interaction and Determination of the Binding Constant in the System "NPFe₃O₄+OVA"

To study the mechanism of interaction of Fe₃O₄ nanoparticles with OVA, stationary spectrofluorometric titration was performed based on the intrinsic

fluorescence of OVA.³¹ The process of fluorescence quenching of OVA titrating NPFe₃O₄ is shown in Fig. 2b. OVA has three tryptophan (Trp) residues,^{16,25} which can become more accessible when the protein structure changes under the influence of external factors (temperature, solvents, chemicals, nanoparticles, etc.). The OVA spectrum presents an intense, a broad band

with an absorption maximum at 335 nm (excitation at 280 nm) (Fig. 2b). The introduction of NPFe_3O_4 into the system leads to a decrease in the intensity of the intrinsic fluorescence of the protein and a shift of the emission band to the blue region by 7 nm,^{26,27} which indicates a chemical interaction between OVA and Fe_3O_4 nanoparticles, as well as some changes in the protein structure.^{9,26} The formation of the “ $\text{NPFe}_3\text{O}_4 + \text{OVA}$ ” complex can be described as an interaction (6):



which is characterized by the complex formation constant or binding constant (7):

$$K_a = [L_nP] / [P][L]^n, \quad (7)$$

where $[P]$ is the concentration of OVA; $[L]$ – NPFe_3O_4 concentration; n is the number of binding centers or seats in the protein molecule.

During the formation of the OVA complex with NPFe_3O_4 , connections occur that keep NPFe_3O_4 in the active center. Such connections, depending on the spatial and chemical environment of the interacting molecules, can be expressed by 4 types of non-covalent interactions: van der Waals forces, hydrogen bonds, electrostatic and hydrophobic interactions.

The mechanism of the observed fluorescence quenching effect can be due to: a dynamic process, a static process, or a combination of both of these processes. Usually, the Stern-Volmer equation (8) is used for the mathematical expression of the extinguishing mechanism:

$$\frac{F_0}{F} = 1 + K_q \tau_0 [Q] = 1 + K_{sv} [Q], \quad (8)$$

where F_0 and F are fluorescence intensity in the absence and presence of a quencher, K_q is the molecular quenching rate constant ($2.0 \times 10^{10} \text{ L} \cdot \text{mol}^{-1} \cdot \text{s}^{-1}$), τ_0 is the average lifetime of a fluorescent molecule in an excited state in the absence of quenchers ($1 \times 10^{-8} \text{ s}$), $[Q]$ is the quencher concentration, the product $k_q \cdot \tau_0 = K_{sv}$ – the Stern-Volmer constant or the quenching constant – in the case of a static quenching mechanism $K_{sv} = K_a$.

It follows from equation (8) that the dependence graph $F_0/F = f[Q]$ (Stern-Volmer graph) is a straight line, the angle coefficient of which is equal to the damping constant K .²⁷ If there is one type of quenching, the graph in the Stern-Volmer coordinates (variant SV) has a linear character; and deviates upward from the linear dependence – in the case of joint action of static and dynamic damping. In our case (Fig. 3a), the SV variant is not linear in nature, *i.e.*, when NPFe_3O_4 interacts with OVA, both dynamic and static types of quenching are observed. The binding constant (K_b) was calculated according to the formula (9):

$$\log \frac{F_0 - F}{F} = n \log K_b + n \log \left(\frac{1}{[Q] - \frac{(F_0 - F)[P]_T}{F_0}} \right) \quad (9)$$

where K_b is the binding constant, n is the number of binding centers, $[P]_T$ is the total concentration of OVA.

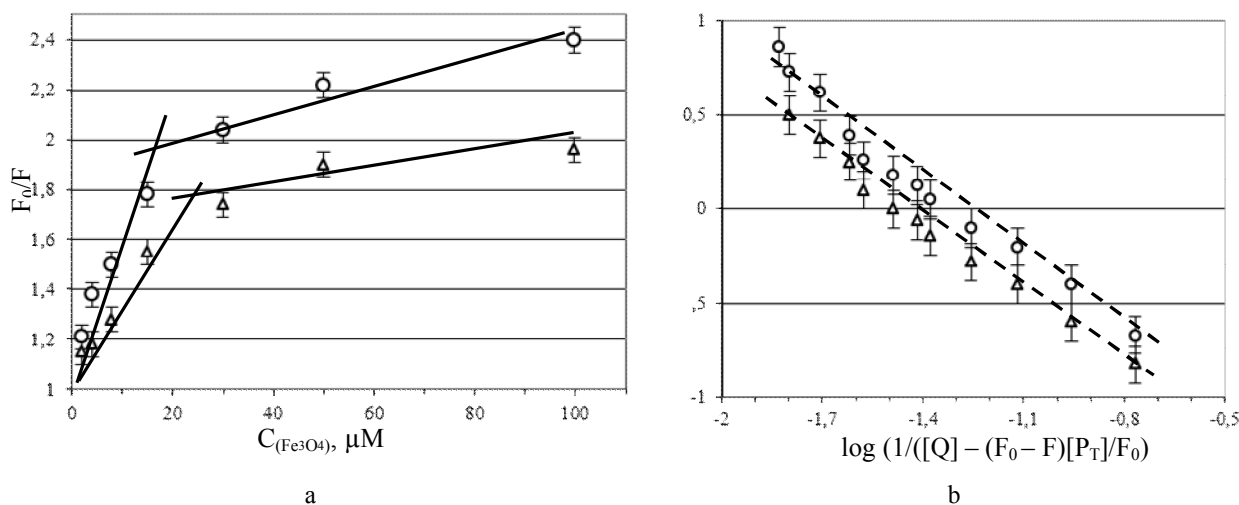


Fig. 3. Fluorescence quenching of OVA (2 μM) at NPFe_3O_4 concentrations: 2, 4, 8, 15, 30, 50, 100 μM , at $\text{pH}=4.6$ and temperature: -296 K and -311 K : a – in the coordinates of the modified Stern–Volmer (Stern–Volmer variant – SV); b is a double logarithmic curve for calculating constant binding

On the basis of data from the graphical images of equations (8) and (9) (Fig. 3a-b), the binding parameters K_{sv} , K_b , n ²⁶ were calculated, while two independent values

of K_{sv}' were calculated at concentrations of NPFe_3O_4 from 0 to 15 μM and K_{sv}'' at concentrations of NPFe_3O_4 from 15 to 100 μM (Fig. 3a; Table 3). Since, $K_{sv} = K_q \cdot \tau_0$, it was

determined that at 296 K and NPFe_3O_4 concentration $\leq 15 \mu\text{M}$ $K_{q1}=3.47 \times 10^{12} \text{L}\cdot\text{mol}^{-1}\cdot\text{s}^{-1}$ at $\text{pH}=4.6$ and $K_{q1}=2.90 \times 10^{12} \text{L}\cdot\text{mol}^{-1}\cdot\text{s}^{-1}$ at $\text{pH}=7.4$ (Table 3). The calculated value of K_{q1} significantly exceeds the maximum quenching constant ($1.0 \times 10^{10} \text{L}\cdot\text{mol}^{-1}\cdot\text{s}^{-1}$),³⁵ which indicates a static quenching mechanism. After increasing the NPFe_3O_4 concentration to more than $15 \mu\text{M}$ – $K_{q2}=3.32 \times 10^{10} \text{L}\cdot\text{mol}^{-1}\cdot\text{s}^{-1}$ at $\text{pH}=4.6$ and $K_{q2}=2.91 \times$

$\times 10^{10} \text{L}\cdot\text{mol}^{-1}\cdot\text{s}^{-1}$ at $\text{pH}=7.4$ (Table 3), which indicates that at high concentrations of NPFe_3O_4 K_{q2} is about $10^{10} \text{L}\cdot\text{mol}^{-1}\cdot\text{s}^{-1}$ and therefore the mechanism of the quenching process is dominated by a static character in the presence of a small number of dynamic collisions. Table 3 shows the results of calculating the constants of the Stern-Volmer equation at different pH and temperature values, as well as the correlation coefficient (R^2).

Table 3. Parameters of Stern-Volmer binding in the system “ NPFe_3O_4 +OVA” in different conditions (pH, temperature) and correlation coefficient

Quencher	pH	Temperature, K	Stern-Volmer parameters				
			K_{SV} , $\text{L}\cdot\text{mol}^{-1}$		R^2	K_q ($\times 10^{12} \text{L}\cdot\text{mol}^{-1}\cdot\text{s}^{-1}$)	
			K_{SV1} ($\times 10^4$)	K_{SV2} ($\times 10^3$)		K_{q1} ($\times 10^{12}$)	K_{q2} ($\times 10^{10}$)
NPFe_3O_4	4.6	296	4.97±0.23	5.84±0.24	0.9986	3.47±0.26	3.32±0.32
		311	3.98±0.17	4.28±0.19	0.9997	2.97±0.21	2.84±0.29
	7.4	296	3.91±0.16	4.86±0.21	0.9965	2.90±0.19	2.91±0.31
		311	2.98±0.11	3.18±0.15	0.9955	1.96±0.18	2.27±0.14

* Note. Data represent the mean \pm standard deviation of three experiments ($n=3$).

It is known that during dynamic quenching, the value of the constant K_{sv} increases with increasing temperature due to a greater number of collisions between the fluorophore (OVA) and the quencher (NPFe_3O_4) due to an increase in the diffusion coefficient. In the process of decreasing K_{SV} and K_q parameters, the static quenching prevails, since higher temperatures affect the stability of the “fluorophore + quencher” complex (in our case, the “OVA+ NPFe_3O_4 ” complex).

As can be seen from the Table 3, the values of K_{sv} and K_q parameters decrease with increasing temperature regardless of pH. Thus, the process of interaction between NPFe_3O_4 and OVA occurs mainly by the mechanism of static quenching, based on the formation of a non-fluorescent nanocomplex.^{9,26,27}

According to Y. Shu *et al.* at the value of the bimolecular quenching rate constant $Kq \square 2.0 \times 10^{10} \text{L}\cdot\text{mol}^{-1}\cdot\text{s}^{-1}$, the dynamic quenching occurs, and at higher values of Kq , the static quenching mechanism prevails.²⁸ Data in the Table 3 shows that the values of Kq ranged from $2.27 \times 10^{10} \text{L}\cdot\text{mol}^{-1}\cdot\text{s}^{-1}$ to $3.47 \times 10^{12} \text{L}\cdot\text{mol}^{-1}\cdot\text{s}^{-1}$, and thus the processes of interaction of NPFe_3O_4 with OVA took place, mainly by the mechanism of static quenching. The decrease in K_{SV} values with increasing pH is associated with the effect of an acidic environment on the main Trp residues, which leads to a decrease in the coagulation of the protein structure, and accordingly promotes the processes of penetration and interaction of Fe_3O_4 nanoparticles.²⁹ The bimolecular quenching rate constant was calculated using the OVA protein lifetime value of 0.1 ns .²⁷ The obtained values are $\sim 10^{12}$, which is 2 orders of magnitude higher than in the purely dynamic

quenching mechanism involving oxygen,³⁰ which is considered to be the largest possible value for aqueous solutions. Therefore, in the studied system, the fluorescence quenching of OVA can be associated with the formation of an intermolecular nanocomplex in the ground state (*i.e.*, a static mechanism), but not due to collision processes, as in the dynamic quenching.⁹

3.1.4.3. Degree of Interaction of NPFe_3O_4 with OVA

An important parameter of the interaction of Fe_3O_4 nanoparticles with OVA is their affinity, which can be estimated using the values of the binding constant (K_b) and the number of centers (n) occupied by NPFe_3O_4 in the structure of OVA. On the surface of NPFe_3O_4 there are oppositely charged structure-forming centers (^{+TM}Fe) and (^{-TM}O). Due to the presence of electromagnetic properties of Fe_3O_4 nanoparticles, the polarization of chemical molecules (H_2O , OVA, *etc.*) increases. As a result, there is an additional ordering of dipoles in the near-surface layer of Fe_3O_4 particles and an increase in adsorption.^{4,9,10}

Thus, the total charge of NPFe_3O_4 depends on pH and, therefore, the mechanism of their interaction with OVA depends on the concentration of H^+ cations in the solution. That is, in an aqueous solution, NPFe_3O_4 exists in the form of four different forms with different degrees of protonation depending on pH: $\text{H}_3\text{Fe}_3\text{O}_4^+$, $\text{H}_2\text{Fe}_3\text{O}_4$, HFe_3O_4^- and $[\text{Fe}_3\text{O}_4(\text{OH})]^{2-}$, while the pK_a values of NPFe_3O_4 are different. Each of these forms exhibits acid-base duality and has different overall charges: at $\text{pH}<6.1$, the positive charge will predominate, the neutral form ($\text{H}_2\text{Fe}_3\text{O}_4$) predominates at $6.1<\text{pH}<7.0$, while for the

existence of the anionic form (HFe_3O_4^-) required pH range=7.1...9. Finally, the dianionic form $[\text{Fe}_3\text{O}_4(\text{OH})]^{2-}$ exists at $\text{pH}>10$. Therefore, the interaction of NPFe_3O_4

with protein depends on the presence of the protonated form. Table 4 shows the binding and thermodynamic parameters of NPFe_3O_4 interaction with OVA.

Table 4. Binding and thermodynamic parameters of NPFe_3O_4 interaction with OVA under different conditions (pH and temperature)

Structure former	pH	Temperature K	Binding parameters		R^2	Thermodynamic parameters		
			Binding constant, K_b ($\times 10^5 \text{L}\cdot\text{mol}^{-1}$)	The number of binding centers, n		ΔG , $\text{kJ}\cdot\text{mol}^{-1}$	ΔH , $\text{kJ}\cdot\text{mol}^{-1}$	ΔS , $\text{J}\cdot\text{mol}^{-1}$
NPFe_3O_4	4.6	296	4.81 ± 0.19	1.02 ± 0.12	0.9966	-29.87 ± 1.62	-51.97 ± 4.12	-171 ± 7.32
		311	4.28 ± 0.16	0.89 ± 0.11	0.9962	-33.83 ± 1.76		
	7.4	296	3.63 ± 0.14	0.98 ± 0.10	0.9960	-28.65 ± 1.52		
		311	3.26 ± 0.13	0.64 ± 0.09	0.9959	-32.98 ± 1.73		

* Note. Data represent the mean \pm standard deviation of three experiments ($n=3$).

As can be seen from the data in the Table 4, the binding constant (K_b) of NPFe_3O_4 with OVA decreases due to the mechanism of static quenching with increasing pH.³¹ In an acidic environment, the α -helix of the secondary structure of OVA changes to a rarer folded “ β -sheet” structure according to D. Kang *et al.*,³² which makes OVA amino acids more accessible to structure-builders and promotes the interaction process of NPFe_3O_4 with OVA, which leads to an increase in K_b . In an alkaline medium, NPFe_3O_4 and OVA have a negative charge, and therefore the interaction is less favorable due to some repulsion between OVA and NPFe_3O_4 . In addition, as the temperature increases, the K_b value of the OVA/ NPFe_3O_4 system decreases, which is associated with changes in the tertiary structure of OVA and a decrease in the affinity of NPFe_3O_4 to OVA at a temperature of 311 K, compared to a temperature of 296 K. Also, during the interaction of NPFe_3O_4 with OVA, the number of centers binding (n) on OVA is: at 296 K – $n=0.98\dots 1.02$, and at 311 K – $n=0.64\dots 0.89$, that is, it decreases. The decrease in the number of available binding sites on OVA for NPFe_3O_4 with increasing temperature is associated with temperature-induced changes in the tertiary structure of OVA, which leads to the formation of a more extended conformation of the main chain of OVA and, therefore, to the displacement of available binding amino acid residues.

The calculated values of n are in the range of 0.64...1.02, which indicates an equimolecular interaction between NPFe_3O_4 and the OVA macromolecule (~ 1:1).

3.1.5. Thermodynamic Parameters of the Interaction Process of NPFe_3O_4 with OVA

The formation of the “ NPFe_3O_4 +OVA” complex is a thermodynamic process, so the value and sign of the thermodynamic parameters (change in Gibbs free energy, ΔG° ; change in enthalpy, ΔH° and change in entropy, ΔS°) provide important information about the nature of the interaction between OVA and NPFe_3O_4 .

The interaction between OVA and NPFe_3O_4 macromolecules can be carried out due to hydrogen bonds, van der Waals forces, ionic and hydrophobic interactions. According to thermodynamic parameters: if the values of ΔH° and ΔS° are negative, then hydrogen bonds and Van der Waals electrostatic forces are the dominant interactions between OVA and NPFe_3O_4 ; with positive values of ΔH° and ΔS° , hydrophobic interactions prevail in the binding process; with negative ΔH° and positive ΔS° , electrostatic interactions are responsible for new and additional bonds between OVA and NPFe_3O_4 ; at a constant value of ΔH° and ΔS° in the studied temperature range – the values of ΔH° and ΔS° can be determined from the Van't-Hoff equation³³ according to equation (10):

$$\ln K_b = \frac{-\Delta G^\circ}{RT} = \frac{-\Delta H^\circ}{RT} + \frac{\Delta S^\circ}{R}, \quad (10)$$

where K_b is the binding constant at a given temperature (T); R is a universal gas constant. According to equation (10), the dependence graph of $\ln K_b = f(T^{-1} \times 10^{-3})$ is a straight line with a slope of ΔH° and at the point of intersection – ΔS° (Fig.4). The values of ΔG° were determined from the Gibbs-Helmholtz equation (11):

$$\Delta G^\circ = \Delta H^\circ - T\Delta S^\circ \quad (11)$$

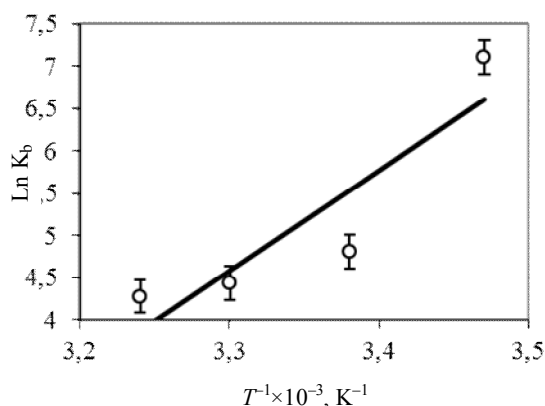


Fig. 4. Graphic expression of Van't Hoff equation

The results of ΔH° , ΔS° and ΔG° calculations are shown in Table 4 and have negative values for the process of binding NPFe_3O_4 to OVA. A negative change in enthalpy (ΔH°) with a negative change in entropy (ΔS°) is observed in many associative processes and is associated with the presence of specific interactions of hydrogen bonds and van der Waals electrostatic forces. In addition, the negative change in enthalpy (ΔH°) indicates that the bonding process is accompanied by heat release (is exothermic), that is, the processes of formation of new bonds prevail over the breaking of individual bonds; and the negative change in entropy (ΔS°) occurs due to the fact that H_2O dipoles (oriented in relation to NPFe_3O_4 and OVA) acquire a more ordered configuration as a result of binding. The negative value of ΔG° indicates that the process of interaction of NPFe_3O_4 with OVA proceeds spontaneously.

It can be concluded that the interaction of NPFe_3O_4 with OVA is carried out due to hydrogen bonds and electrostatic coordination interactions, which is consistent with the mechanism of interaction of iron nanoparticles, iron oxides with various types of proteins, proposed by a number of authors.^{4,9,10,34}

Thus, the nature of nanoparticles plays an important role in the processes of interaction with proteins, which is determined by pH and chemical composition of the technological environment, which affects the properties and chemical surface activity of nanoparticles, in particular, the oxide nature – NPFe_3O_4 . The acidity of the aqueous environment and solvation of the surface of nanoparticles determine the way of interaction with protein molecules, and the nature, structure, and dispersion of nanoparticles determine the degree of conformational changes of the protein.

3.2. Justification of the Mechanism of Water Binding and Water Retention by Fe_3O_4 Nanoparticles in Protein-Containing Systems

3.2.1. Scientific Substantiation of the H_2O Binding Mechanism by Nanoparticles of Fe_3O_4

The surface chemical activity of NPFe_3O_4 is determined mainly by electrostatic: dipole-dipole (van-der-vaalis) and ion-dipole interactions.^{4,5,12} In the adsorption of protein molecules, in particular, OVA and H_2O , coordination and hydrogen bonds are involved on the surface of NPFe_3O_4 . This slows the formation of hydrophobic bonds between macromolecules, which prevents their aggregation and increases the stability of the system: “protein+solvated NPFe_3O_4 ”.^{4,10} Under the influence of Fe_3O_4 nanoparticles, protein molecules

undergo structural changes. “Clusters” and “loops” of protein chains are formed due to electrostatic interactions of protein molecules (OVA) with NPFe_3O_4 (Fig. 5).

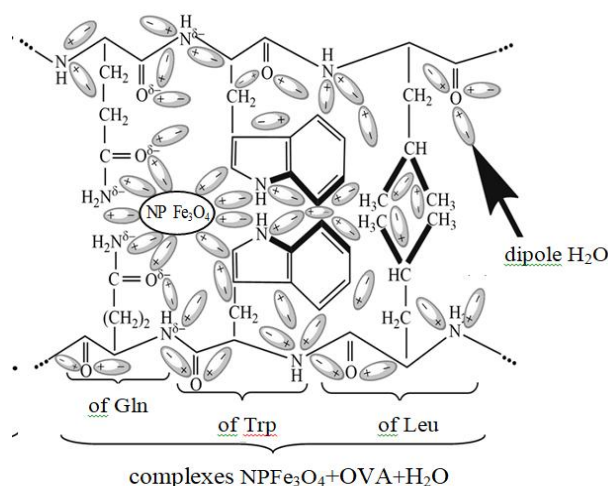


Fig. 5. Electrostatic complex NPFe_3O_4 with “ $\text{H}_2\text{O}+\text{OVA}$ ”

The electrostatic binding of H_2O molecules is observed in the surface layer of polar particles Fe_3O_4 and in “clusters” and in “loops” of OVA chains. H_2O molecules at the expense of hydrogen bonds form a solvato associate “ $\text{H}_2\text{O}+\text{NPFe}_3\text{O}_4+\text{OVA}$ ”, which is characterized by sufficient stability. This increases the water binding and water retention of protein-containing systems.

3.2.2. Experimental Confirmation of Water Binding and Water Retention by Fe_3O_4 Nanoparticles. Determination of the Binding Forms of H_2O with Nanoparticles of Fe_3O_4

Fe_3O_4 particles are characterized by a rather homogeneous distribution in diameter ($<d \leq 80$ nm), close to monodispersion (Fig. 6).

Ultrafine dispersion determines the ability of NPFe_3O_4 to sorption and hydration. At the same time, there is a shift towards chemically bound moisture compared to the free form of H_2O . The water-binding capacity of NPFe_3O_4 is confirmed by indicator and thermographic methods: the amount of bound water is (92.2–93.1) % and free water is (6.9–7.8) % (Fig. 7).

In polyphasic systems containing biopolymers, NPFe_3O_4 and water, water binding and water-holding capacities are exercised due to the structure-forming and stabilizing properties of components, in particular NPFe_3O_4 particles. It has been experimentally established that in technological media (milk, whey, kefir, solutions of NaCl and sucrose) at $\text{pH}=6.0$; 4.5 NPFe_3O_4 has a high hydration capacity, which increases with increasing temperature (Table 5).

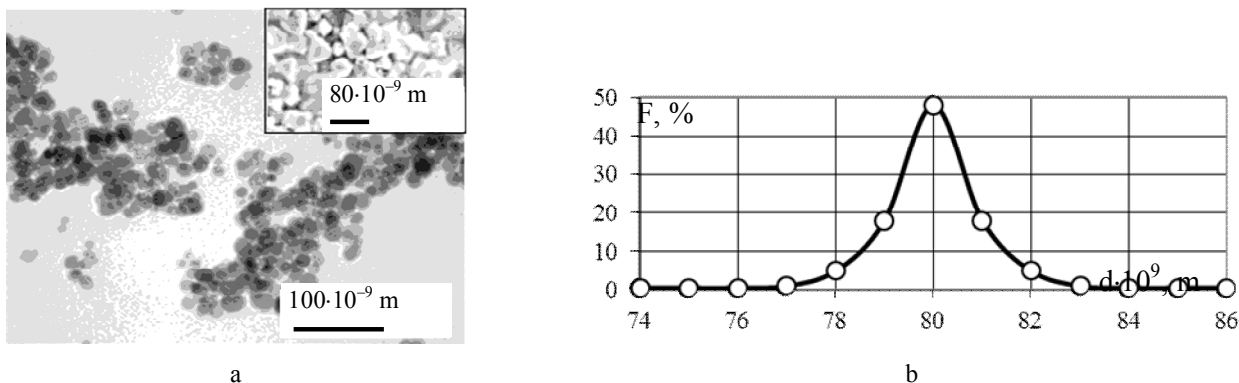


Fig. 6. Microstructure (a) and diameter distribution (b) of particles $\text{NPF}_3\text{O}_4^{12}$

Table 5. Water absorption coefficients of NPF_3O_4 in different environments

Polar environment	Water absorption coefficients, relative units	
	$T=293\pm 5\text{K}$	$T=323\pm 8\text{K}$
Sodium bicarbonate, pH=6.0	12.4 ± 0.4	12.8 ± 0.4
Ethanoic acid solution, pH=4.5	12.8 ± 0.4	13.0 ± 0.4
Sodium chloride solution, 0.5 %	13.1 ± 0.5	13.4 ± 0.5
Sodium chloride solution, 1.7 %	13.4 ± 0.5	13.5 ± 0.5
Sucrose solution, 1.1 %	13.6 ± 0.5	13.7 ± 0.5
Sucrose solution, 5.0 %	13.8 ± 0.5	14.0 ± 0.5
Milk	12.6 ± 0.4	12.9 ± 0.4
Kefir	12.4 ± 0.4	12.5 ± 0.4
Syvorotka	13.2 ± 0.4	13.6 ± 0.4

* Note. Data represent the mean \pm standard deviation of three experiments ($n=3$).

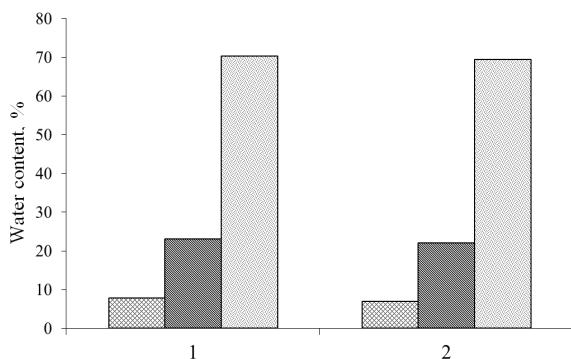


Fig. 7. Distribution of water in the NPF_3O_4 after swelling determined by: 1 – thermogravimetric method; 2 – chemogravimetric method: \square – amount of physico-chemically bound moisture, %; \blacksquare – the amount of physically and mechanically bound moisture, %; \square – amount of free moisture, %

The pronounced hydrophilic properties and the propensity of NPF_3O_4 to form aqua associates are associated with high dispersion and active specific surface area of Fe_3O_4 particles with polarized centers. These factors increase the intensity of hydration NPF_3O_4 : the swelling coefficient reaches its maximum value after 30 min, $K_n = (345-355)\%$, and water absorption capacity after 30 min increases by (1.9–2.1) times.^{10,19}

4. Conclusions

1. The mechanism of interaction of Fe_3O_4 nanoparticles with H_2O and OVA is substantiated:

- the ability of NPF_3O_4 for self-organization into electrostatic complexes with OVA due to the formation of hydrogen bonds, van der Waals forces, and electrostatic coordination interactions was noted;

- it was established that the acidity of the aqueous medium and the surface solvation of Fe_3O_4 nanoparticles determine the way of interaction with protein molecules, and the nature, structure, dispersion of NPF_3O_4 determine the degree of protein conformational changes;

- it was established that in polyphase systems containing proteins (OVA), H_2O , etc., the water-binding and water-holding capacity of NPF_3O_4 is adjusted due to the “clusterophilicity” and the ability of nanoparticles to polarize, electrostatic coordination, and the formation of aqua-associates;

2. The mechanism of interaction of Fe_3O_4 nanoparticles with H_2O and OVA was experimentally confirmed:

- chemisorption of OVA and H_2O on the surface of NPF_3O_4 was proven by the IR-Fourier spectroscopy method: new absorption bands appear, and some characteristics of absorption bands shift to lower frequencies;

– the study of the dynamic dispersion of the light established an increase in the ζ -potential of the OVA/NPFe₃O₄ dispersed system by 1.89...1.92 times compared to OVA. At the same time, the ζ -potential of the OVA/NPFe₃O₄ system has rather high values of 33.2...34.9 mV – this means the possibility of stabilizing dispersed systems based on proteins with Fe₃O₄ nanoparticles. An increase in the hydrodynamic size of particles relative to the nominal ($\langle d \rangle$ 70 nm) NPFe₃O₄ in the aqueous solution to 77...78 nm is shown, which is associated with the presence of the H₂O molecule on the surface of NPFe₃O₄; and due to chemisorption of OVA indicates an increase in the size of particles in the OVA/NPFe₃O₄ system to 75.3...76.2 nm;

– the elemental composition of the investigated samples was studied by the energy dispersive X-ray spectroscopy: NPFe₃O₄, OVA and “OVA+ NPFe₃O₄”. As a result, the process of adsorption and chemical interaction of Fe₃O₄ nanoparticles with OVA was confirmed;

– spectrofluorometric studies established that the process of interaction between NPFe₃O₄ and OVA takes place mainly by the mechanism of static quenching, based on the formation of an intermolecular (non-fluorescent) nanocomplex in the ground state, and not due to collision processes, as in the dynamic quenching. The Stern-Volmer binding parameters of NPFe₃O₄ with OVA were determined: binding constant (K_b) at 296 K: – $4.81 \times 10^5 \text{ L} \cdot \text{mol}^{-1}$ (pH=4.6) and $3.63 \times 10^5 \text{ L} \cdot \text{mol}^{-1}$ (pH=7.4); at 311 K: – $4.28 \times 10^5 \text{ L} \cdot \text{mol}^{-1}$ (pH=4.6) and $3.26 \times 10^5 \text{ L} \cdot \text{mol}^{-1}$ (pH=7.4); the number of binding centers (n) is in the range of 0.64...1.02, which indicates that the interactions between NPFe₃O₄ and the OVA macromolecule occur in a ratio of ~1:1;

– thermodynamic calculations show that NPFe₃O₄ interacts with OVA due to hydrogen bonds and electrostatic coordination interactions;

– a sufficiently high hydration capacity of NPFe₃O₄ in various polar environments has been established (the maximum value of the swelling coefficient is $K_n=345...355$ %);

– indicator and thermogravimetric analysis determined the forms of H₂O connection with NPFe₃O₄ after swelling: the amount of bound water is (92.2–93.1) %, free – (6.9–7.8) %.

The obtained results will make it possible to model the processes of water binding and water retention in various technological environments, stabilization processes of polyphase systems, functional and technological characteristics of protein-containing compositions, and quality indicators of finished products.

It should be noted that it is of practical interest to study the processes of chemisorption of various biopolymers (proteins of various origins, lipoproteins, carbohydrates, etc.) on the surface of Fe₃O₄ nanoparticles;

mechanisms of formation of the microstructure of polyphase systems with the addition of NPFe₃O₄, water binding, water retention, stabilization.

References

- [1] Dron, I.; Nosova, N.; Fihurka, N.; Bukartyk, N.; Nadashkevych, Z.; Varvarenko, S.; Samaryk, V. Investigation of Hydrogel Sheets Based on Highly Esterified Pectin. *Chem. Chem. Technol.* **2022**, *16*, 220-226. <https://doi.org/10.23939/chcht16.02.220>
- [2] Goralchuk, A.; Gubsky, S.; Omelchenko, S.; Riabets, O.; Grinchenko, O.; Fedak, N.; Kotlyar, O.; Cheremskaya, T.; Skrynnyk, V. Impact of Added Food Ingredients on Foaming and Texture of the Whipped Toppings: A Chemometric Analysis. *Eur. Food Res. Technol.* **2020**, *246*, 1955-1970. (In Ukrainian) <https://doi.org/10.1007/s00217-020-03547-3>
- [3] Bratychak, M.; Zemke, V.; Chopyk, N. The features of Rheological and Tribological Behavior of High-Viscosity Polyolefine Compositions Depending on their Content. *Chem. Chem. Technol.* **2021**, *15*, 486-492. <https://doi.org/10.23939/chcht15.04.486>
- [4] Tsykhanovska, I.; Evlash, V.; Alexandrov, A.; Lazarieva, T.; Svidlo, K.; Gontar, T.; Yurchenko, L.; Pavlotska, L. Substantiation of the Mechanism of Interaction between Biopolymers of Rye-and-wheat Flour and the Nanoparticles of the Magnetofood. Food Additive in Order to Improve Moisture-retaining Capacity of Dough. *East.-Eur. J. Enterp. Technol.* **2018**, *2/11* (92), 70-80. (In Ukrainian) <https://doi.org/10.15587/1729-4061.2018.126358>
- [5] Tsykhanovska, I.; Evlash, V.; Oleksandrov, O.; Gontar, T. Mechanism of Fat-Binding and Fat-Contenting of the Nanoparticles of a Food Supplement on the Basis of Double Oxide of Two- and Trivalent Iron. *Ukr. Food J.* **2018**, *7*, 702-715. <https://doi.org/10.24263/2304-974X-2018-7-4-14>
- [6] Jumadilov, T.; Malimbayeva, Z.; Yskak, L.; Suberlyak, O.; Kondarov, R.; Imangazy, A.; Agibayeva, L.; Akimov, A.; Khimersen, K.; Zhuzbayev, A. Comparative Characteristics of Polymethacrylic Acid Hydrogel Sorption Activity in Relation to Lanthanum Ions in Different Intergel Systems. *Chem. Chem. Technol.* **2022**, *16*, 418-431. <https://doi.org/10.23939/chcht16.03.418>
- [7] Li, J.; Pylpynchuk, I.; Johansson, D.; Kessler, V.; Seisenbaeva, G.; Langton, M. Self-Assembly of Plant Protein Fibrils Interacting with Superparamagnetic Iron Oxide Nanoparticles. *Scientific Reports* **2019**, *9*, 8939. <https://doi.org/10.1038/s41598-019-45437-z>
- [8] Chavali, M.; Nikolova, M. Metal Oxide Nanoparticles and their Applications in Nanotechnology. *SN Applied Sciences* **2019**, *1*, 607. <https://doi.org/10.1007/s42452-019-0592-3>
- [9] Tsykhanovska, I.; Stabnikova, O.; Gubsky, S. Spectroscopic Studies of Interaction of Iron Oxide Nanoparticles with Ovalbumin Molecules. *Mater. Proc* **2022**, *9(1)*, 2. <https://doi.org/10.3390/materproc2022009002>
- [10] Tsykhanovska, I.; Evlash, V.; Blahyi, O. Mechanism of Water-Binding and Water-Retention of Food Additives Nanoparticles Based on Double Oxide of Two- and Trivalent Iron. *Ukr. Food J.* **2020**, *9*, 298-321. <https://doi.org/10.24263/2304-974x-2020-9-2-4>
- [11] Tsykhanovska, I.; Evlash, V.; Alexandrov, A.; Gontar, T. Dissolution Kinetics of Fe₃O₄ Nanoparticles in the Acid Media. *Chem. Chem. Technol.* **2019**, *13*, 170-184. <https://doi.org/10.23939/chcht13.02.170>
- [12] Tsykhanovska, I.; Evlash, V.; Alexandrov, A.; Gontar, T.; Shmatkov, D. The Study of the Interaction Mechanism of Linoleic

- Acid and 1-Linoleyl-2-oleoyl-3-linolenoyl-glycerol with Fe₃O₄ Nanoparticles. *Chem. Chem. Technol.* **2019**, *13*, 303-316. <https://doi.org/10.23939/chcht13.03.303>
- [13] Ramachandrabai, K.; Choi, M.; Hong, G. Micro- and Nano-Scaled Materials for Strategy-Based Applications in Innovative Livestock Products: A Review. *Trends Food Sci Technol* **2018**, *71*, 25. <https://doi.org/10.1016/j.tifs.2017.10.017>
- [14] Zozulya, G.; Kuntiy, O.; Mnykh, R.; Sozanskyi, M. Synthesis of Antibacterially Active Silver Nanoparticles by Galvanic Replacement on Magnesium in Solutions of Sodium Polyacrylate in an Ultrasound. *Chem. Chem. Technol.* **2021**, *15*, 493-499. <https://doi.org/10.23939/chcht15.04.493>
- [15] Deivasigamani, P.; Ponnusamy, S.; Sathish, S.; Suresh, A. Superhigh Adsorption of Cadmium(ii) Ions onto Surface Modified Nano Zerovalent Iron Composite (cns-nzvi): Characterization, Adsorption Kinetics and Isotherm Studies. *Chem. Chem. Technol.* **2021**, *15*, 457-464. <https://doi.org/10.23939/chcht15.04.457>
- [16] Dantas, M.; Tenório, H.; Lopes, T.; Pereira, H.; Marsaioli, A.; Figueiredo, I.; Santos, J. Interactions of Tetracyclines with Ovalbumin, the Main Allergen Protein from Egg White: Spectroscopic and Electrophoretic Studies. *Int. J. Biol. Macromol.* **2017**, *102*, 505-514. <https://doi.org/10.1016/j.ijbiomac.2017.04.052>
- [17] Kashanian, F.; Habibi-Rezaei, M.; Bagherpour, A.; Seyedarabi, A.; Moosavi-Movahedi, A. Magnetic Nanoparticles as Double-Edged Swords: Concentration-Dependent Ordering or Disordering Effects on Lysozyme. *RSC Adv.* **2017**, *7*, 54813. <https://doi.org/10.1039/C7RA08903A>
- [18] Babu, S.; Neeraja, D. Experimental Study of Natural Admixture Effect on Conventional Concrete and High Volume Class F Flyash Blended Concrete. *Case Stud. Constr. Mater.* **2016**, *6(C)*, 43-62. <https://doi.org/10.1016/j.cscm.2016.09.003>
- [19] Tsykhanovska I., Evlash V., Alexandrov O., Riabchykov M., Lazarieva T., Nikulina A., Blahyi O. Technology of Bakery Products Using Magnetofood as a Food Additive. In *Bioenhancement and Fortification of Foods for a Healthy Diet*; Paredes-López, O.; Shevchenko, O.; Stabnikov, V.; Ivanov, V., Eds.; CRC Press: Boca Raton, FL, 2022. <https://doi.org/10.1201/9781003225287>
- [20] Hussein, S.; Amir, Z.; Jan, B.; Khalil, M.; Azizi, A. Colloidal Stability of CA, SDS and PVA Coated Iron Oxide Nanoparticles (IONPs): Effect of Molar Ratio and Salinity. *Polymers* **2022**, *14*, 4787. <https://doi.org/10.3390/polym14214787>
- [21] Maestro, A.; Santini, E.; Zabiegaj, D.; Llamas, S.; Ravera, F.; Liggieri, L.; Ortega, F.; Rubio, R.; Guzman, E. Particle and Particle-Surfactant Mixtures at Fluid Interfaces: Assembly, Morphology, and Rheological Description. *Adv. Condens. Matter Phys.* **2015**, *2015*, ID 917516. <https://dx.doi.org/10.1155/2015/917516>
- [22] Dzwolak, W.; Kato, M.; Taniguchi, Yo. Fourier Transform Infrared Spectroscopy in High-Pressure Studies on Proteins. *Biochimica et Biophysica Acta (BBA) – Protein Structure and Molecular Enzymology* **2002**, *1595*, 131-144. [https://doi.org/10.1016/S0167-4838\(01\)00340-5](https://doi.org/10.1016/S0167-4838(01)00340-5)
- [23] Byler, D.; Susi, H. Examination of the Secondary Structure of Proteins by Deconvolved FTIR Spectra. *Biopolymers* **1986**, *25*, 469-487. <https://doi.org/10.1002/bip.360250307>
- [24] Midoux, P.; Wahl, P.; Aucht, J.; Monsigny, M. Fluorescence Quenching of Tryptophan by Trifluoroacetamide. *Biochim. Biophys. Acta-Gen. Subj.* **1984**, *801*, 16-25. [https://doi.org/10.1016/0304-4165\(84\)90207-1](https://doi.org/10.1016/0304-4165(84)90207-1)
- [25] Stein, P.; Leslie, A.; Finch, J.; Carrell, R. Crystal Structure of Uncleaved Ovalbumin at 1.95 Å Resolution. *J. Mol. Biol.*, **1991**, *221*, 941-959. [https://doi.org/10.1016/0022-2836\(91\)80185-W](https://doi.org/10.1016/0022-2836(91)80185-W)
- [26] Lin, T.; Shu, L.; Hongna, B.; Xin, G. Interaction of Cyanidin-3-O-glucoside with Three Proteins. *Food Chem.* **2016**, *196*, 550-559. <https://doi.org/10.1016/j.foodchem.2015.09.089>
- [27] Lakowicz, J. *Principles of Fluorescence Spectroscopy*; Third Edition; Springer: New York, 2006. <https://doi.org/10.1007/978-0-387-46312-4>
- [28] Shu, Y.; Xue, W.; Xu, X.; Jia, Z.; Yao, X.; Liu, S.; Liu, L. Interaction of Erucic Acid with Bovine Serum Albumin Using a Multi-Spectroscopic Method and Molecular Docking Technique. *Food Chem.* **2015**, *173*, 31-37. <https://doi.org/10.1016/j.foodchem.2014.09.164>
- [29] Bhattacharya, M.; Mukhopadhyay, S. Structural and Dynamical Insights into the Molten-Globule Form of Ovalbumin. *J. Phys. Chem. B*, **2012**, *116*, 520-531. <https://doi.org/10.1021/jp208416d>
- [30] Blank-Shim, S.; Schwaminger, S.; Borkowska-Panek, M.; Anand, P.; Yamin, P.; Fraga-García, P.; Fink, K.; Wenzel, W.; Berensmeier, S. Binding Patterns of Homo-Peptides on Bare Magnetic Nanoparticles: Insights into Environmental Dependence. *Scientific Reports* **2017**, *7*, 14047. <https://doi.org/10.1038/s41598-017-13928-6>
- [31] Bi, S.; Song, D.; Tian, Y.; Zhou, X.; Liu, Z.; Zhang, H. Molecular Spectroscopic Study on the Interaction of Tetracyclines with Serum Albumins. *Spectrochim. Acta Part A* **2005**, *61*, 629-636. <https://doi.org/10.1016/j.saa.2004.05.028>
- [32] Kang, D.; Ryu, S.; Park, Y.; Czarnik-Matusiewicz, B.; Jung, Y. PH-Induced Structural Changes of Ovalbumin Studied by 2D Correlation IR Spectroscopy. *J. Mol. Struct.* **2014**, *1069*, 299-304. <https://doi.org/10.1016/j.molstruc.2014.02.061>
- [33] Ghalandari, B.; Divsalar, A.; Saboury, A.; Parivar, K. The New Insight into Oral Drug Delivery System Based on Metal Drugs in Colon Cancer Therapy Through β-Lactoglobulin/oxali-palladium Nanoparticles. *J. Photochem. Photobiol. B*, **2014**, *140*, 255-265. <https://doi.org/10.1016/j.jphotobiol.2014.08.003>
- [34] Zhang, H.; Wu, P.; Zhu, Z.; Wang, Y. Interaction of γ-Fe₂O₃ Nanoparticles with Fibrinogen. *Spectrochim Acta A Mol Biomol Spectrosc.* **2015**, *151*, 40-47. <https://doi.org/10.1016/j.saa.2015.06.087>

Received: January 26, 2023 / Revised: February 27, 2023 / Accepted: April 05, 2023

ФІЗИКО-ХІМІЧНІ ДОСЛІДЖЕННЯ МЕХАНІЗМУ ВЗАЄМОДІЇ НАНОЧАСТИНОК ПОДВІЙНОГО ОКСИДУ ДВО- ТА ТРИВАЛЕНТНОГО ФЕРУМУ З СЕРПШОВИМ БІЛКОМ-ОВАЛЬБУМІНОМ І ВОДОЮ

Анотація. Новизною роботи є теоретичне обґрунтування й експериментальне підтвердження механізму взаємодії наночастинок Fe₃O₄ з H₂O та овальбуміном-OVA, що проведено за допомогою комплексу фізико-хімічних досліджень. Визначено, що механізм ґрунтується на кластерофільності наночастинок і водневих, електростатичних і ван-дер-ваальсових взаємодіях. Встановлено, що взаємодія наночастинок Fe₃O₄ з OVA відбувалася за механізмом статичного гасіння з утворенням міжмолекулярного нефлуоресцентного комплексу, який змінює нативну структуру OVA. Константа зв'язування змінювалася від 3,3×10⁷ до 4,8×10⁵ л·моль⁻¹ залежно від значення рН середовища та температури. Термодинамічними розрахунками підтверджено спонтанність процесу зв'язування з переважанням ентальпійного фактора.

Ключові слова: наночастинок Fe₃O₄, вода, OVA, хемосорбція, акваасоціація.